

Generation of relativistic electrons at the termination shock in the solar flare region

G. Mann¹, A. M. Veronig², and F. Schuller¹

¹ Leibniz-Institut für Astrophysik Potsdam, An der Sternwarte 16, D-14482 Potsdam, Germany; GMann@aip.de

² Institute of Physics, University of Graz, Universitätsplatz 5, A-8010 Graz, Austria

Accepted: April 2024

ABSTRACT

Context. Solar flares are accompanied by an enhanced emission of electromagnetic waves from the radio up to the γ -ray range. The associated hard X-ray and microwave radiation is generated by energetic electrons. These electrons play an important role, since they carry a substantial part of the energy released during a flare. The flare is generally understood as a manifestation of magnetic reconnection in the corona. The so-called standard CSHKP model is one of the most widely accepted models for eruptive flares. The solar flare event on September 10, 2017 offers us a unique opportunity to study this model. The observations from the Expanded Owens Valley Solar Array (EOVSA) show that $\approx 1.6 \times 10^4$ electrons with energies > 300 keV are generated in the flare region.

Aims. There are signatures in solar radio and extreme ultraviolet (EUV) observations as well as numerical simulations that a “termination shock” (TS) appears in the magnetic reconnection outflow region. Electrons accelerated at the TS can be considered to generate the loop-top hard X-ray sources. In contrast to previous studies, we investigate whether the heating of the plasma at the TS provides enough relativistic electrons needed for the hard X-ray and microwave emission observed during the solar X8.2 flare on September 10, 2017.

Methods. We studied the heating of the plasma at the TS by evaluating the jump in the temperature across the shock by means of the Rankine-Hugoniot relationships under coronal circumstances measured during the event on September 10, 2017. The part of relativistic electrons was calculated in the heated downstream region.

Results. In the magnetic reconnection outflow region, the plasma is strongly heated at the TS. Thus, there are enough energetic electrons in the tail of the electron distribution function (EDF) needed for the microwave and hard X-ray emission observed during the event on September 10, 2017.

Conclusions. The generation of relativistic electrons at the TS is a possible mechanism of explaining the enhanced microwave and hard X-ray radiation emitted during flares.

Key words. Sun: corona – Sun: flares – Sun: acceleration of particles – shock waves

1. Introduction

On the Sun, a flare occurs as a sudden enhancement of the local emission of electromagnetic waves covering the whole spectrum from the radio up to the γ -ray range with a duration of minutes to hours (see Aschwanden (2005) as a textbook). During flares, a large amount of stored magnetic energy is suddenly released and transferred into the local heating of the coronal plasma, mass motions (as e.g., jets and coronal mass ejections (CMEs)), and the generation of energetic particles (usually called solar energetic particle (SEP) events) (see e.g., Heyvaerts 1981; Lin 1974; Reames, Barbier, & Ng 1996; Klein & Trottet 2001). The flare is considered to be a manifestation of magnetic reconnection in the corona. Presently, it is widely under-

stood in terms of the so-called standard or CSHKP model (Carmichael 1964; Sturrock 1966; Hirayama 1974; Kopp & Pneumann 1976) that was developed to explain eruptive flares; that is, flares associated with a CME. According to the CSHKP model, a filament is rising up due to its photospheric footpoint motions, leading to the stretching of the underlying magnetic field lines and, subsequently, to the establishment of a current sheet. If the current within this sheet exceeds a critical value, plasma waves are excited due to different plasma instabilities, leading to an enhancement of the resistivity (see e.g., Treumann & Baumjohann (1997)). Then, magnetic reconnection can take place in the region of enhanced resistivity, which is called the “diffusion region.” Due to the strong curvature of the magnetic field lines in the vicinity of the diffusion region, the plasma slowly inflowing into the reconnection

site is shooting away from the diffusion region, forming the outflow region.

The generation of energetic electrons during flares is of special interest, since they carry a substantial part of the energy released during flares (Lin & Hudson 1971, 1976; Emslie et al. 2004, Krucker et al. 2010, Krucker & Battaglia 2014). Observations with the Reuven Ramaty High Energy Solar Spectroscopic Imager (RHESSI) (Lin et al. 2002) reveal that 10^{36} electrons with energies beyond 30 keV are typically produced per second during X-class flares (Warmuth et al. 2007). There are several models for electron acceleration in the present debate (see e.g., Chapter 11 in the textbook by Aschwanden (2005) as well as Zharkova et al. (2011) and Mann (2015) as reviews). One of them is electron acceleration at the so-called “termination shock” (TS). If the velocity of the plasma in the outflow region becomes super-Alfvénic, a shock wave can be established. For instance, it can happen due to the interaction of the outflow jet with the underlying loops. Numerical simulations (Forbes 1986, 1988; Forbes & Malherbe 1986, Workman et al. 2011; Takasao et al. 2015; Takasao & Shibata 2016; Takahashi et al. 2017; Shen et al. 2018; Kong et al. 2019; Cai et al. 2021) support the establishment of a TS in the magnetic reconnection outflow region. Masuda et al. (1994), Shibata et al. (1995), and Tsuneta & Naito (1998) reported on so-called loop-top sources of the hard X-ray radiation. Tsuneta & Naito (1998) proposed that the TS could be the source of energetic electrons, which are needed for the hard X-ray emission that can explain these loop-top sources. Solar radio (Aurass et al. 2002; Aurass & Mann 2004; Chen et al. 2015) and extreme ultraviolet (EUV) (Polito et al. 2018; Cai et al. 2021) observations revealed signatures of such TSs in flare regions. Mann et al. (2006, 2009) and Warmuth et al. (2009) discussed the generation of energetic electrons at the TS by “shock drift acceleration” (SDA). In contrast to these studies, here we investigate whether the heating of the plasma at the TS provides enough of the relativistic electrons needed for the microwave and hard X-ray emission during flares.

To do that, we investigate the X8.2 flare that occurred on September 10, 2017. The event took place on the western solar limb and was associated with a fast CME. It exhibits various characteristics of a textbook event following the CSHKP scenario, like the formation of a hot flux rope, an indication of magnetic reconnection jets, and signatures of a large-scale hot current sheet beneath the eruption (e.g., Cheng et al. 2018, Veronig et al. 2018, Warren et al. 2018). Therefore, this event offers us an excellent opportunity to study the flare scenario. Chen et al. (2020) measured the plasma parameters as the electron number density, the magnetic field, the temperature, and the number density of relativistic electrons in the flare region by employing microwave imaging observations with the newly commissioned Expanded Owens Valley Solar Array (EOVSA; Gary et al. 2018). They found that the microwave-emitting energetic electrons are strongly concentrated in the loop-top region. The presence of a TS

there could be a possible explanation. Hence, these measurements allow us to determine both the plasma parameters at the TS and the number density of electrons with energies > 300 keV. These values were used to demonstrate that the heating of the plasma at the TS provides enough energetic electrons needed for the microwave and hard X-ray emission during flares.

In Section 2, the properties of the TS are derived by evaluating the Rankine-Hugoniot relationships under special circumstances in the flare region. The observational results measured by the EOVSA instrument (Gary et al. 2018) during the solar flare on September 10, 2017 (Chen et al. 2020) are presented in Section 3. Whether the heating of the plasma at the TS can provide enough of the relativistic electrons with energies > 300 keV needed for the observed microwave and X-ray radiation are discussed in Section 4. The results of the paper are summarized in Section 5.

2. Properties of the termination shock

The TS is considered to be a nearly perpendicular shock (Tsuneta & Naito 1998, Mann et al. 2006, 2009). It is confirmed by numerical simulations (see e.g., Fig. 1e in Kong et al. (2019)). In magnetohydrodynamics (MHD), shock waves are described in terms of the so-called Rankine-Hugoniot relationships (see e.g., Priest (1982); here, we followed the approach given in Appendix A in the paper by Mann et al. (2018)). The shock normal, \mathbf{n}_s , is directed along the x axis; in other words, the shock itself is located in the y-z plan (see Fig. 1). The magnetic field, \mathbf{B} , is put in the x-z plane and takes an angle, θ , to the x axis in the upstream region. All of the quantities with the subscript 1 or 2 denote those in the upstream and downstream regions, respectively. These Rankine-Hugoniot relationships were evaluated for the special case of a nearly perpendicular, fast-mode shock – $\theta \rightarrow 90^\circ$ – leading to

$$\frac{B_2}{B_1} = X \quad (1)$$

(see Eq. (A.9) in Mann et al. (2018) for the jump in the magnetic field) and

$$\frac{T_2}{T_1} = 1 + \frac{(\gamma - 1)}{2} \cdot \frac{v_{A1}^2}{c_{s1}^2} \cdot (M_A)^2 \cdot \left(1 - \frac{1}{X^2}\right) \quad (2)$$

(see Eq. (A.8) in Mann et al. (2018) for the jump in the temperature). Here, $X = \rho_2/\rho_1$ denotes the jump in the mass density across the shock. The mass density, ρ , is related to the full particle number density, N , by $\rho = \tilde{\mu} m_p N$ (m_p , proton mass; $\tilde{\mu} = 0.6$, mean molecular weight (Priest 1982)). The equation of state, $p = N k_B T$ (k_B , Boltzmann’s constant), relates the pressure, p , to the full particle number density, N , and the temperature, T . Here, the Alfvén velocity and sound speed are given by $v_{A1} = B_1/(4\pi\rho_1)^{1/2}$ and $c_{s1} = (\gamma k_B T_1/\tilde{\mu} m_p)^{1/2}$ (γ , ratio of the specific heats) in the upstream region, respectively. In the flare region, $v_{A,1} \gg c_{s,1}$ can be assumed, as is shown

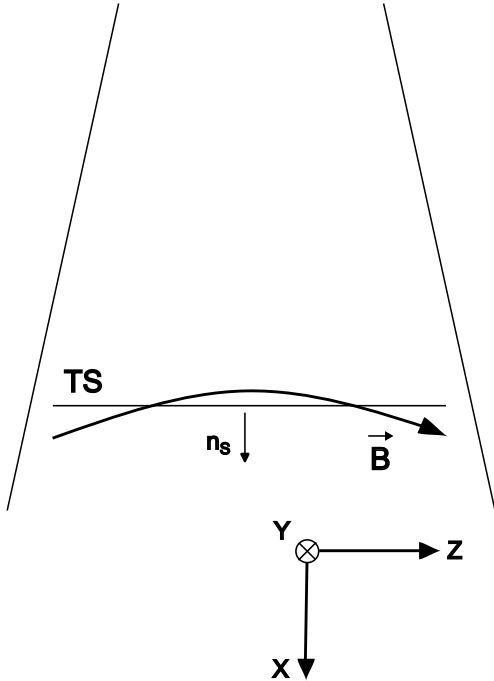


Fig. 1. Sketch of the magnetic reconnection outflow region with the TS. The upstream and downstream regions of the TS are located above and below the TS, respectively. The coordinate system employed in the paper is also drawn.

in Section 4. Then, according to the Rankine-Hugoniot relationships, the Alfvén-Mach number $M_A = v_s/v_{A1}$ of the shock is related to the density jump, X , by

$$M_A = \sqrt{X \cdot \frac{[\gamma + X(2 - \gamma)]}{[(\gamma + 1) - X(\gamma - 1)]}} \quad (3)$$

(see Eq. (A.10) in Mann et al. (2018)) with the shock speed, v_s .

The TS is a fast magnetosonic shock that is connected with positive jumps in the mass density, the magnetic field, and the temperature. Now, we look to the jump of the temperature at the TS (see Eq. (2)). Crucially, it depends on the ratio $v_{A,1}/c_{s1}$. This ratio is $\gg 1$ in flare regions, as is discussed in Section 4. Hence, the plasma is strongly heated from the temperature in the upstream region, T_1 , up to a temperature in the downstream region of the TS, T_2 , under special circumstances in flare regions. Thus, it could be that there are relativistic electrons in the tail of the electron distribution function (EDF) in the downstream region. Next, we calculated the part of electrons with energies beyond an energy, E^* , in the downstream EDF.

To do that, we assumed a Maxwellian EDF in the downstream regions with temperature T_2 :

$$f_M(\mathbf{p}) = C_M \cdot e^{-E_{kin}/k_B T_2}. \quad (4)$$

Microwave and hard X-ray observations during the flare on September 10, 2017 reveal that the EDF in the loop-top region consists of a thermal core and a broken power law in the energetic tail (see Fig. 3c in Chen et al. (2021) and the third paragraph of Sect. 3). Such an EDF is described by several parameters as the temperature of the thermal core as well as the break energy and the power law indices of the broken power law. In contrast to such an EDF, a Maxwellian one has only one parameter, namely the temperature. Unfortunately, the parameters of a broken power law cannot be determined by macroscopic relationships such as, for example, the equation of momentum. Since the Rankine-Hugoniot relationships result from the macroscopic MHD equations, these relations do not allow one to derive any information about the change in the parameters of the broken power law across the shock, such as the power law indices, for instance. For these reasons and for simplicity's sake, we chose a Maxwellian EDF in the downstream region, since it has only the temperature, T , as the parameter and the Rankine-Hugoniot relationships provide information about the jump in the temperature across the shock.

In order to derive the differential electron number density, we followed the approach presented in the paper by Mann (2018). The kinetic energy, E_{kin} , of an electron with the momentum, p ($p = \|\mathbf{p}\|$), is given by $E_{kin} = (p^2 c^2 + m_e^2 c^4)^{1/2} - m_e c^2$ (m_e , electron mass). The constant, C_M , can be fixed to

$$\frac{1}{C_M} = 4\pi(m_e c)^3 \cdot \int_0^\infty d\epsilon \cdot \sqrt{\epsilon(2 + \epsilon)} \cdot (1 + \epsilon) \cdot e^{-\epsilon/\epsilon_{th}} \quad (5)$$

(see Eq. (3.14) in Mann (2018)), with $\epsilon = E_{kin}/m_e c^2$ and $\epsilon_{th} = k_B T_2/m_e c^2$, if the EDF is normalized to unity. Then, the number density, $N_e(\epsilon^*)$, of electrons with energies beyond E^* is found to be

$$\frac{N_e(\epsilon^*)}{N_{e,0}} = 4\pi(m_e c)^3 C_M \cdot \int_{\epsilon^*}^\infty d\epsilon \cdot \sqrt{\epsilon(2 + \epsilon)} \cdot (1 + \epsilon) \cdot e^{-\epsilon/\epsilon_{th}}, \quad (6)$$

with $\epsilon^* = E^*/m_e c^2$ and $N_{e,0}$ as the complete electron number density. Then, the differential electron number density defined by

$$\frac{dN_e(E)}{dE} = \frac{1}{m_e c^2} \cdot \frac{dN_e}{d\epsilon} \quad (7)$$

results from Eq. (6) as

$$\frac{dN_e(E)}{dE} = \frac{4\pi(m_e c)^3 C_M}{m_e c^2} \cdot \sqrt{\epsilon(2 + \epsilon)} \cdot (1 + \epsilon) \cdot e^{-\epsilon/\epsilon_{th}} \quad (8)$$

in the case of a Maxwellian EDF with temperature T_2 .

3. Solar flare on September 10, 2017

The solar event on September 10, 2017 was an X8.2 flare and the second-largest one in solar cycle 24. Since it appeared at the limb, it is an unique event through which to study the flare scenario in an excellent manner. It was described in detail from different points of view (Veronig et

al. 2018; Warren et al. 2018; Gary et al. 2018; Longcope et al. 2018; Hayes et al. 2019; Morosan et al. 2019; Chen et al. 2020; Yu et al. 2020; French et al. 2020; Reeves et al. 2020; Fleishman et al. 2020, 2022). This event confirms well the standard (CSHKP) flare model. It showed an erupting flux rope with a CME and an underlying current sheet. The event was also accompanied by an SEP event (Guo et al. 2018) and a long-lasting (≈ 12 hours) γ -ray emission with energies > 100 MeV (Omodei et al. 2018).

In this event, signatures of a long hot current sheet were observed behind the erupting flux rope (Seaton & Darnel 2018; Warren et al. 2018, Yan et al. 2018) in the flare region. This led to the formation of a large-scale reconnection current sheet (RCS). The microwave spectral imaging observations with the EOVSA instrument (Gary et al. 2018) reveals that relativistic electrons are present in the region between the erupting flux rope and the underlying flare loop arcade (Chen et al. 2020). Inspection of Figure 2a in Chen et al. (2020) shows that the RCS extends in the height range of 20-70 Mm in projection above the limb. Chen et al. (2020) identified the RCS as a bright feature in the 193 Å band. It was observed by the “Atmospheric Imaging Assembly” (AIA, Lemen et al. 2012) instrument on board the “Solar Dynamics Observatory” (SDO, Pesnel et al. 2012). The 193 Å band is sensitive for hot plasmas with a temperature of about 18 MK. Figure 3a in Chen et al. (2020) reveals that the X and Y points are located at heights of ≈ 32 Mm and ≈ 20 Mm above the limb in projection, respectively. According to numerical simulations (Forbes 1986, 1988; Forbes & Malherbe 1986, Workman et al. 2011; Takasao et al. 2015; Takasao & Shibata 2016; Takahashi et al. 2017; Shen et al. 2018, Kong et al. 2019), the TS is predicted in the region between the Y point and the underlying flare loop arcade. Hence, the TS is expected in the height region of about 20 Mm in the event on September 10, 2017. There, an enhanced hard X-ray radiation is observed. The hard X-ray source observed by the RHESSI spacecraft (Lin et al. 2002) is located at the top of the flare loop arcade with a FWHM size of $\approx 20'' \times 30''$ (or 14.5 Mm \times 21.8 Mm) (see Figs. (1a) and (1d) in Chen et al. (2021)). There, the number density of electrons with energies beyond 300 keV is much greater, as is shown in Figure 3e in Chen et al. (2020). That is an indication that the TS could be the source of these relativistic electrons, as was proposed by Tsuneta & Naito (1998).

The microwave data of the EOVSA instrument (Gary et al. 2018) and the hard X-ray data of the RHESSI instruments allow one to derive the EDF at the loop-top source of this event. Chen et al. (2021) did that for a broad energy range, 10 keV – 1 MeV, during the early impulsive phase of the flare by means of the forward fitting method (Holman et al. 2003). The resulting EDF consists of a thermal core with a temperature of ≈ 25 MK, a broken power law in the energetic tail beyond ≈ 16 keV, and an electron power law index of ≈ 3.6 . Beyond ≈ 160 keV, the power law breaks to a power law with an index of ≈ 8.5 (see Fig. 3c in Chen et al. (2021)).

The upstream and downstream regions of the TS are located in the regions between the Y point and the TS and between the TS and the flare loop arcade, respectively. There, we find a temperature of $T_1 = 18$ MK in the upstream region (see Fig. 2a in Chen et al. (2020) and also Warren et al. (2018)) as well as an electron number density, $N_{e,2} = 10^{10}$ cm $^{-3}$, and magnetic field, $B_2 = 400$ G (see Fig. 3b in Chen et al. (2020)), in the downstream region as the plasma parameters at the TS. Furthermore, the number density of electrons with energies > 300 keV is found to be $\approx 1.6 \times 10^4$ cm $^{-3}$ (because of $\log[N_{e,>300keV}(cm^{-3})] = 4.2$ in Fig. 3e in Chen et al. (2020)) below the Y point.

4. Discussion

The aim of this section is to show that the heating of the plasma at the TS provides enough relativistic electrons in the downstream region of the TS by employing data from the solar event on September 10, 2017 (see Sect. 3).

As was mentioned in Section 3, the temperature $T_1 = 18$ MK (corresponding to an energy of 1.55 keV) is found in the upstream region of the TS. It results in a sound speed of $c_{s,1} = (\gamma k_B T_1 / \tilde{\mu} m_p)^{1/2} = 643$ km s $^{-1}$ for $\gamma = 5/3$. Furthermore, a magnetic field strength of $B_2 = 400$ G and an electron number density of $N_{e,2} = 10^{10}$ cm $^{-3}$ are adopted in the downstream region, leading to an Alfvén velocity of $v_{A,2} = B_2 / (4\pi \tilde{\mu} m_p N_2)^{1/2} = 8128$ km s $^{-1}$ for $\tilde{\mu} = 0.6$ (Priest 1982).¹ Thus, the ratio $v_{A,2}/c_{s,1} = 12.6$ – the assumption that $(v_{A,2}/c_{s,1})^2 \gg 1$ to derive Eq. (3) – is well justified.

Next, the ratio T_2/T_1 had to be calculated by means of Eq. (2). Inserting Eq. (3) for M_A in Eq. (2) and taking into account $v_{A,1} = v_{A,2}/X^{1/2}$, one gets

$$\frac{T_2}{T_1} = 1 + \frac{1}{6} \cdot \frac{v_{A,2}^2}{c_{s,1}^2} \cdot \frac{(X^2 - 1)(5 + X)}{X^2(4 - X)}. \quad (9)$$

The jump in the temperature, T_2/T_1 , across the TS increases from one to infinity if X changes from one to four. It is calculated for several values of the density jump, X , varying in the range of 1.1-1.6 by means of Eq. (9) and $v_{A,2}/c_{s,1} = 12.6$. The results are summarized in Table 1. Additionally, the electron number density, $N_{e,1}$, the magnetic field, B_1 , and the Alfvén velocity, $v_{A,1}$, of the upstream region are also listed in Table 1. The sixth column reveals that the plasma is strongly heated across the TS. The thermal energies in the downstream region, $k_B T_2$, are given in the sixth column of Table 1. They vary from 16.7 keV to 70.9 keV for a TS with Alfvén-Mach numbers, M_A , in the range of 1.10-1.60, respectively.

Since the plasma is heated in the downstream region, a Maxwellian EDF was assumed there for simplicity’s sake (see also the discussion in Sect. 2). The number density of electrons with energies beyond 300 keV, $N_{e,2>300keV}$, was

¹ In the coronal plasma, the full particle number N density is related to the electron number density N_e by $N = 1.92N_e$ (Mann et al. 1999).

Table 1. Parameters of the TS according to the Rankine-Hugoniot relationships for density jumps, X , in the range of 1.1-1.6 for the plasma conditions measured during the solar event on September 10, 2017, i.e., the temperature, $T_1 = 18$ MK, in the upstream region as well as the electron number density, $N_{e,2} = 10^{10} \text{ cm}^{-3}$, and the magnetic field, $B_2 = 400$ G, in the downstream region. The Alfvén-Mach number, M_A (second column), was calculated with Eq. (3). $N_{e,1} = N_{e,2}/X$ (third column), $B_1 = B_2/X$ (fourth column), and $v_{A,1} = v_{A,2}/X^{1/2}$ (fifth column) are obtained for the electron number density, the magnetic field, and the Alfvén velocity, respectively, in upstream regions of the TS. The temperature in the downstream region, T_2 , was determined by Eq. (9). The corresponding thermal energies, $k_B T_2$, are given in the sixth column. In the upstream region, a temperature of $T_1 = 18$ MK leads to a thermal energy of $k_B T_1 = 1.55$ keV. $N_{e,2>300\text{keV}}/N_{e,2}$ (seventh column) and $N_{e,2>20\text{keV}}/N_{e,2}$ (eighth column) denote the ratios between the number density of electrons with energies beyond 300 keV and 20 keV, respectively, and the full electron number density in the downstream region, $N_{e,2}$. They were calculated by means of Eq. (6), with $\epsilon_{300\text{keV}}^* = 0.5859$ and $\epsilon_{20\text{keV}}^* = 0.0391$.

X	M_A	$N_{e,1}(10^{10}\text{cm}^{-3})$	$B_1(\text{G})$	$v_{A,1}(\text{km s}^{-1})$	$k_B T_2(\text{keV})$	$N_{e,2>300\text{keV}}/N_{e,2}$	$N_{e,2>20\text{keV}}/N_{e,2}$
1.10	1.076	0.9091	364	7757	16.7	5.451×10^{-8}	0.511
1.11	1.083	0.9009	360	7707	18.0	4.870×10^{-7}	0.554
1.12	1.091	0.8929	357	7677	19.4	1.536×10^{-6}	0.578
1.13	1.099	0.8850	354	7646	20.7	3.871×10^{-6}	0.606
1.20	1.153	0.8333	333	7412	29.5	2.497×10^{-4}	0.737
1.30	1.232	0.7692	308	7136	41.1	3.677×10^{-3}	0.830
1.40	1.313	0.7143	286	6876	51.6	1.444×10^{-2}	0.876
1.50	1.396	0.6667	267	6645	61.5	3.360×10^{-2}	0.904
1.60	1.483	0.6250	250	6426	70.9	5.971×10^{-2}	0.923

calculated with Eq. (6) for different values of the density jump, X , in the range of 1.1-1.6, as is presented in the seventh column in Table 1. We note that the EDF was treated in a fully relativistic manner in Section 2. The measurements with EOVSAs (Gary et al. 2018) during the solar event on September 10, 2017 provide $N_{e,2>300\text{keV}} = 1.58 \times 10^4 \text{ cm}^{-3}$ (see Section 3 and Fig. 3e in Chen et al. (2020)) or $N_{e,2>300\text{keV}}/N_{e,2} = 1.58 \times 10^{-6}$ for $N_{e,2} = 10^{10} \text{ cm}^{-3}$. Inspecting Table 1, such a value of $N_{e,2>300\text{keV}}/N_{e,2}$ is found for a TS with a density jump of 1.12 and an Alfvén-Mach number of 1.09. Thus, the TS with these special parameters is able to heat the downstream plasma from 1.55 keV up to 19.4 keV, and hence to explain the production of relativistic electrons during the solar event on September 10, 2017.

The TS considered is a low Alfvén-Mach number shock. Adopting the plasma parameters in the upstream region of the TS as derived here (see Table 1), the upstream flow has a velocity of $v_{TS} = 8342 \text{ km s}^{-1}$. At the TS, which is a fast magnetosonic shock, the kinetic energy of the upstream flow is transformed into an increase in the temperature (heating) and the magnetic field in the downstream region (see Priest (1982)). This flow carries a total energy density of $w_{total} = w_{kin} + w_{mag} = 1.027 \times 10^4 \text{ erg cm}^{-3}$, with a kinetic energy density of $w_{kin} = N_{e,1} m_p v_{TS}^2 / 2 = 5.198 \times 10^3 \text{ erg cm}^{-3}$ and a magnetic energy density of $w_{mag} = B_1^2 / 8\pi = 5.071 \times 10^3 \text{ erg cm}^{-3}$. Hence, an energy of ≈ 641 keV is available for each electron. This result demonstrates that the inflow in the

upstream region contains enough energy to produce energetic electrons up to relativistic energies by means of heating at a low Alfvén-Mach number shock (such as $M_A = 1.09$, for instance).

To illustrate this, Figure 2 shows the differential electron number density of this special TS in the downstream (full line) and upstream regions (dashed line). It reveals that the electrons are strongly energized up to relativistic energies at the transition through the TS. There is a pronounced part of relativistic energies in the downstream region in the event under study. 58 % of all electrons reach energies beyond 20 keV (see the eighth column in Table 1). This result agrees with the EOVSAs observations (Fleishmann et al. 2022) and confirms that the energetic electrons carry a substantial part of the energy released during flares (Lin & Hudson 1971, 1976; Emslie et al. 2004, Krucker et al. 2010, Krucker & Battaglia 2014). Chen et al. (2021) derived electron energy spectra for the event on September 10, 2017 by means of a combined analysis of hard X-ray and microwave data measured by RHESSI (Lin et al. 2002) and EOVSAs (Gary et al. 2018), respectively. Figure 3c in Chen et al. (2021) shows the differential electron number density (thick black curve) for the impulsive phase of this event. It consists of a thermal (i.e., Maxwellian) core and a broken power law in the energetic tail. Figure 3c in Chen et al. (2021) and Figure 2 of this paper are presented on the same scale. The comparison of these figures reveals that the differential electron number density resulting from the heating at the TS (see full line in Fig. 2) agrees roughly with the differential electron density obtained from the observations (thick black curve

² The thermal energy density can be neglected with respect to the other ones.

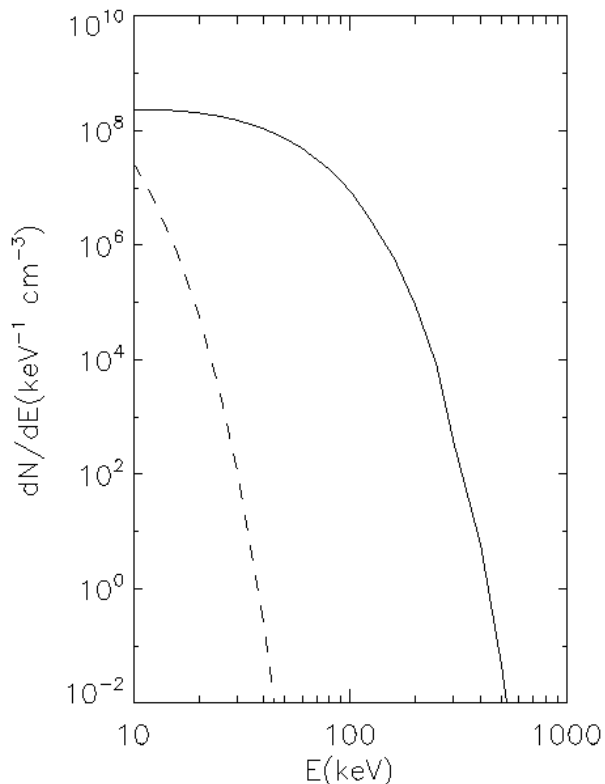


Fig. 2. Energy dependence of the differential electron number density, dN_e/dE , for plasma with a thermal energy of 1.55 keV ($\epsilon_{th,1} = 0.0030$ and $N_{e,1} = 8.929 \times 10^9 \text{ cm}^{-3}$; dashed line) and 19.4 keV ($\epsilon_{th,2} = 0.0379$ and $N_{e,2} = 10^{10}$; full line) according to Eq. (8).

of Fig. 3c in Chen et al. (2021)). We note that Chen et al. (2021) derived a broken power law for the differential electron number density, whereas the heating at the TS results in a Maxwellian EDF. (With respect to this subject, we refer to the discussion in Section 2.)

Previously, Mann et al. (2006, 2009) and Warmuth et al. (2009) proposed the generation of energetic electrons at the TS by SDA. It is well known that SDA immediately produces a beam-like EDF (Mann et al. 2018) in the upstream region of the shock. In contrast to these studies, here we demonstrate using the example of the September 10, 2017 flare that the heating of the plasma across the TS provides enough energetic electrons up to the relativistic energies needed for the microwave and hard X-ray emission. The resulting EDF is not beam-like as in the case of SDA but has a broad pronounced part at relativistic energies (see Fig. 2).

5. Summary and conclusions

There are signatures of a TS in the magnetic reconnection outflow region in solar radio (Aurass et al. 2002, Aurass & Mann 2004, Chen et al. 2015) and EUV (Polito et al. 2018; Cai et al. 2021) observations as well as numerical

simulations (Forbes 1986, 1988; Forbes & Malherbe 1986, Workman et al. 2011, Takasao & Shibata 2016, Takahashi et al. 2017, Shen et al. 2018, Kong et al. 2019). Tsuneta and Naito (1998) proposed the TS as the source of energetic electrons responsible for the hard X-ray loop-top sources observed in solar flares.

The X8.2 solar flare on September 10, 2017 (Chen et al. 2020) gives us a unique opportunity to study the generation of energetic electrons with observations from the EOVSA instrument (Gary et al. 2018). This event clearly supports the standard (CSHKP) model of eruptive flares. Signatures of a current sheet were identified by Warren et al. (2018) and Chen et al. (2020). Relativistic electrons were produced in the vicinity of this current sheet. A value of 1.6×10^4 electrons per cm^3 with energies > 300 keV was derived from the EOVSA microwave images and spectra in the region between the lower end of the current sheet and the underlying loops; that is, the microwave emitting energetic electrons are strongly concentrated in the loop-top region. This finding can be explained by the presence of a TS in the region between the lower end of the current sheet and the underlying flare loops. The excellent EOVSA data of this event (Chen et al. 2020) allows one to determine the plasma parameters in the upstream and downstream regions of the TS. Adopting these parameters, we investigated the jump in the temperature across the shock by means of the Rankine-Hugoniot relationships (see Table 1). We show that a low Alfvén-Mach number TS with $M_A \approx 1.09$ is able to produce enough of the relativistic electrons needed to explain the microwave radiation measured by the EOVSA instrument in the September 10, 2017 flare. A substantial fraction – namely, 58% – of all electrons gain an energy beyond 20 keV.

In conclusion, the generation of relativistic electrons by heating the plasma at the TS is a possible mechanism of producing energetic electrons up to the relativistic energies needed for microwave and hard X-ray emission during large solar flares. The reason is that a large ratio between the Alfvén velocity and the sound speed upstream of the TS leads to a strong energizing of the downstream plasma.

Acknowledgements. GM and FS express their thanks to the financial support by the Deutsches Zentrum für Luft- und Raumfahrt (DLR) under the grant 50 OT 2304. AMV acknowledges the Austrian Science Fund (FWF) under the grant 10.55776/14555.

References

- Aschwanden, M. J. 2005, Physics of the solar corona (Praxis Publishing Ltd, Chichester, UK)
- Aurass, H. & Mann, G. 2004, ApJ 615, 426
- Aurass, H., Vršnak, B., & Mann, G. 2002, A&A 384, 273
- Cai, Q., Feng, H., Ye, J., & Shen, Ch. 2021, ApJ 912, 79C
- Carmichael, H. 1964, NASA Spec. Pub. 50, 451
- Chen, B., Bastian, T. S., Shen, C., Gary, D. E., Krucker, S. & Glesener, L. 2015, Science 350, 6265, 1238
- Chen, B., Shen, C., Gary, D. E., Reeves, K. K., Fleishman, G. D., Yu, S., Guo, F., Krucker, S., Lin, J., Nita, G. M., & Kong, X. 2020, Nature Astron. 4, 1140

- Chen, B., Battaglia, M., Krucker, S., Reeves, K. K., & Glesener, L. 2021, *ApJL* 908, 55
- Cheng, X., Li, Y., Wan, L. F., Ding, M. D., Chen, P. F., Zhang, J., Liu, J. J. 2018, *ApJ* 866, 64
- Emslie, A. G., Kucharek, H., Dennis, B. R., et al. 2004, *J. Geophys. Res.* 109 (A18), 10104
- Fleishman, G. D., Gary, D. E., Kuroda, N., Yu, S., & Nita, G. M. 2020, *Science* 367, 278
- Fleishman, G. D., Nita, G. M., Chen, b., Yu, S. & Gary, D. E. 2022, *Nature* 606, 674
- French, R. J., Matthews, S. A., van Driel-Gesztelyi, L., Long, D. M., & Judge, P. G. 2020, *ApJ* 900, 192
- Forbes, T. G. 1986, *ApJ* 305, 553
- Forbes, T. G. 1988, *Solar Phys.* 117, 97
- Forbes, T. G. & Malherbe, J. M. 1986, *ApJL* 302, L67
- Gary, D. E., Chen, B., Dennis, B. R. et al. 2018, *ApJ* 863, 83
- Guo, J. Dumbović, M., Wimmer-Schweingruber, R., et al. 2018, *Space Weather* 16, 1156
- Hayes, L. A., Gallagher, P. T., Dennis, B. R., et al. 2019, *ApJ* 875, 33
- Heyvaerts, J. 1981, *Solar Magnetohydrodynamica (Gordon and Breach)*
- Hirayama, T. 1974, *Solar Phys.* 34, 323
- Holman, G. D., Sui, L., Schwartz, R. A., & Emslie, A. G. 2003, *ApJ* 595, L97
- Klein, K.-L. & Trotter, G. 2001, *Space Sci. Rev.* 95, 215
- Kong, X., Guo, F., Shen, C., Chen, B., Chen, Y., Musset, S., Glesener, L., Pongkitiwanichakul, P., & Giacalone, J. 2019, *ApJ*, 887, L37
- Kopp, R. & Pneuman, G. W. 1976, *Solar Phys.* 50, 85
- Krucker, S., Hudson, H. S., Glesener, L., White, S. M., Masuda, S., Wuelser, J.-P. & Lin, R. P. 2010, *ApJ* 714, 1108
- Krucker, S. & Battaglia, M. 2014, *ApJ* 780, 107
- Lemen, J. R., Title, A. M., Akin, D. J., et al. 2012, *Solar Phys.* 275, 17
- Lin, R. P. 1974, *Space Sci. Rev.* 16, 189
- Lin, R. P. & Hudson, H. S. 1971, *Solar Phys.* 17, 412
- Lin, R. P. & Hudson, H. S. 1976, *Solar Phys.* 50, 153
- Lin, R. P., Dennis, B. R., Hurford, G. J. et al. 2002, *Solar Phys.* 210, 3
- Longcope, D., Unverferth, J., Klein, C., McCarthy, M., & Priest, E. 2019, *ApJ* 868, 148
- Mann, G. 2018, *J. Plasma Phys.* 81, 475810601, 1
- Mann, G., Jansen, F., MacDowall, R. J., Kaiser, M. L. & Stone, R. G. 1999, *A&A* 348, 614
- Mann, G., Aurass, H., & Warmuth, A. 2006, *A&A* 454, 969
- Mann, G., Warmuth, A., & Aurass, H. 2009, *A&A* 528, A104
- Mann, G., Melnik, V. N., Rucker, H. O., Konovalenko, A. A. & Brazhenko, A. I. 2018, *A&A* 609, A41
- Masuda, S., Kosugi, T., Hara, H., Tsuneta, S., & Ogawara, Y. 1994, *Nature* 371, 495
- Morosan, D. E., Carley, E. P., Hayes, L. A., et al. 2019, *Nature Astron.* 3, 452
- Omodei, N., Pece-Rollins, M., Longo, F., Allafort, A., & Krucker, S. 2018, *ApJL* 865, L7
- Pesnell, W. P., Thompson, B. J., & Chamberlein, P. C. 2012, *Solar Phys.* 275, 3
- Polito, V. Galan, G., Reeves, K. K., & Musset, S. 2018, *ApJ* 865, 161
- Priest, E. R. 1982, *Solar Magnetohydrodynamics (Dordrecht: Kluwer Academic Publishers)*, 199
- Reames, D. V., Barbier, L. M., & Ng, C. K. 1996, *ApJ* 466, 473
- Reeves, K. K., Polito, V., Chen, B., Galan, G., Yu, S., Liu, W., & Li, G. 2020, *ApJ* 905, 165
- Seaton, D. B. & Darnel, J. M. 2018, *ApJL* 852, L9
- Shen, C., Kong, X., Guo, F. Raymond, J. C., & Chen, B. 2018, *ApJ* 869, 116
- Shibata, K. Mausuda, S., Shimojo, M., et al. 1995, *ApJ* 451, L83
- Sturrock, P. A. 1966, *Nature* 211, 695
- Treumann, R. & Baumjohann, W. 1997, *Advances in Space Plasma Physics (London Imperial College Press)*, 143
- Takahashi, T., Qui, J., & Shibata, K. 2017, *ApJ* 848, 102
- Takasao, S., Matsumoto, T., Nakamura, N., & Shibata, K. 2015, *ApJ* 805, 135
- Takasao, S. & Shibata, K. 2016, *ApJ* 823, 150
- Tsuneta, S. & Naito, T. 1998, *ApJ* 495, L67
- Veronig, A. M., Podladchikova, T., Dissauer, K., et al. 2018, *ApJ* 868, 107
- Warmuth, A., Mann, G., & Aurass, H. 2007, *Central European Astrophys. Bulletin* 31, 135
- Warmuth, A., Mann, G., & Aurass, H. 2009, *A&A* 494, 677
- Warren, H. P., Brocks, D. H., Ugarte-Urra, I., Reep, J. W., Crump, N. A., & Doschek, G. A. 2018, *ApJ* 854, 122
- Workman, J. C., Blackman, E. G., & Ren, C. 2011, *Phys. Pl.* 18, 092902
- Yan, X. L., Yang, L. H., Xue, Z. K., et al. 2018, *ApJL* 853, L18
- Yu, S., Chen, B., Reeves, K. U., Gary, D. E., Musset, S., Fleishman, G. D., Nita, G. M., & Glesener, L. 2020, *ApJ* 900, 17
- Zharkova, V. V., Arzner, K., Benz, A. O., et al. 2011, *Space Sci. Rev.* 159, 357